

# A Halo Occupation Interpretation Of Quasars At $z \sim 1.5$ Using Very Small Scale Clustering Information

S. Eftekharzadeh<sup>1,2</sup>, A. D. Myers<sup>1</sup>, E. Kourkchi<sup>3</sup>, et al.

<sup>1</sup> Department of Physics and Astronomy, University of Wyoming, 1000 University Ave., Laramie, WY 82071

<sup>2</sup> Department of Physics, Southern Methodist University, 3215 Daniel Ave., Dallas, TX 75225

<sup>3</sup> Institute for Astronomy, University of Hawaii, 2680 Woodlawn Drive, Honolulu, HI 96822, USA

10 October 2018

## ABSTRACT

We combine the most precise small scale ( $< 100 \text{ h}^{-1}\text{kpc}$ ) quasar clustering constraints to date with recent measurements at large scales ( $> 1 \text{ h}^{-1}\text{Mpc}$ ) from the extended Baryon Oscillation Spectroscopic Survey (eBOSS) to better constrain the satellite fraction of quasars at  $z \sim 1.5$  in the halo occupation formalism. We build our Halo Occupation Distribution (HOD) framework based on commonly used analytic forms for the one and two-halo terms with two free parameters: the minimum halo mass that hosts a central quasar and the fraction of satellite quasars that are within one halo. Inspired by recent studies that propose a steeper density profile for the dark matter haloes that host quasars, we explore HOD models at kiloparsec scales and best-fit parameters for a range of concentrations. We find that an HOD model with a satellite fraction of  $f_{\text{sat}} = 0.062^{+0.018}_{-0.026}$  and minimum mass of  $M_m = 2.32^{+0.46}_{-0.44} \times 10^{12} \text{ h}^{-1} M_\odot$  for the host dark matter haloes best describes quasar clustering (on all scales) at  $z \sim 1.5$ . Our derived satellite fraction is consistent with recently reported values for quasars at  $z \sim 1.4$  that adopted the same HOD formalism.

**Key words:** cosmology: observations, small-scale clustering, halo occupation; quasars: general, surveys, close pairs

## 1 INTRODUCTION

The advent of the first large, homogeneous surveys of the extra-galactic sky prompted cosmologists to begin to think about galaxies as discrete points embedded in statistical structures (e.g. Neyman, Scott & Zonn 1962; Neyman & Scott 1974). These structures could be characterized in terms of their size, the distribution of the discrete points that occupied them, and their distribution across the wider Universe (see, e.g. Cooray & Sheth 2002, for a review). As it became increasingly clear that dark matter dominated the mass budget in galaxies (e.g. Rood et al. 1972; Ostriker, Peebles & Yahil 1974; Rubin, Thonnard & Ford 1978), it became more natural to think of occupation statistics in terms of the virialized haloes that host luminous tracers (e.g. White & Rees 1978). This line of reasoning ultimately led to empirical approaches that describe how cosmological tracers occupy underlying dark matter structures, such as the Halo Occupation Distribution framework (HOD; e.g., Berlind & Weinberg 2002; Zheng, Coil & Zehavi 2007, and references therein). Parameterizations of the HOD typically consist of a two-halo term, which characterizes how haloes of a certain mass cluster around each other, and a one-halo term that relates galaxy and dark matter statistics through the probability that a halo of a given mass contains a number of galaxies of a given type.

The key observables that are used for constraining HOD de-

scriptions in the common formalism are the number density and the clustering of a given tracer population. As such, the HOD framework has now been successfully used to model galaxy clustering measurements for a wide range of redshifts and galaxy types. Quasars, the most luminous of the Active Galactic Nuclei, are driven by accreting supermassive black holes at the centers of galaxies. It is now well-established that the centers of most galaxies contain a supermassive black hole (e.g. Kormendy & Richstone 1995), and that the evolution of active quasars and inactive galaxies is interrelated (e.g. Kauffmann & Haehnelt 2000). It is therefore reasonable to think of quasars simply as a biased tracer of certain types of galaxies that should also, in theory, be empirically describable using HOD statistics.

In the wake of large spectroscopic surveys such as the 2dF (Folkes et al. 1999) and SDSS (e.g., Fukugita et al. 1996; Gunn et al. 1998; York et al. 2000; Vanden Berk et al. 2001; Stoughton et al. 2002; Strauss et al. 2002; Tegmark et al. 2004; West et al. 2004; Yip et al. 2004a,b; Bolton et al. 2004; Rojas et al. 2005; Wilhite et al. 2005), the clustering of quasars has been measured at a range of redshifts (e.g., Croom et al. 2004; Porciani, Magliocchetti & Norberg 2004; Myers et al. 2006, 2007a,b; Shen et al. 2007, 2009; Ross et al. 2009; Richardson et al. 2012; White et al. 2012; Richardson et al. 2013; Ross et al. 2013; Eftekharzadeh et al. 2015; Laurent et al. 2017). Typically, these studies focus on the large-

scale clustering of quasars via the two-point correlation function, which constrains the “two-halo term” that describes how “central” dark matter haloes cluster around each other. The consensus is that, at most redshifts, quasars occupy central haloes of masses a few times  $10^{12} h^{-1} M_{\odot}$ .

Probing how quasars are distributed within haloes—the so-called “one-halo” term—is trickier, however. As quasars occupy massive haloes, they are rare in general. Further, the haloes that host quasars, particularly at high redshift (e.g., White et al. 2012; Eftekhari et al. 2015), are on the steeply falling part of the halo mass function. This implies that instances of two quasars occupying a single halo at high redshift may be very rare indeed. Finding close pairs of quasars is complicated further by the fact that most large spectroscopic surveys use fiber-fed multi-object spectrographs. Such surveys can have restrictions on how closely fibers can be placed together on the sky, which has prompted follow-up surveys of close quasar pairs using long-slit spectrographs (e.g., Hennawi et al. 2006; Myers et al. 2008; Hennawi et al. 2010; Kayo & Oguri 2012; Eftekhari et al. 2017). These long-slit surveys, in combination with the large-scale two-point correlation function, have been used to constrain the one-halo term for quasars via clustering measurements over a wide redshift range ( $z \sim 0.5\text{--}3$ ) and scale (Richardson et al. 2012; Kayo & Oguri 2012; Shen et al. 2013).

Recent measurements of quasar clustering have used a number of different assumptions for the overall form of the quasar HOD. For instance Kayo & Oguri (2012, henceforth KO12) model both the distribution of satellite and central quasars using Gaussians, ultimately expressing the HOD using two-to-three fitting parameters. On the other hand, Zheng, Coil & Zehavi (2007); Richardson et al. (2012, 2013) and Shen et al. (2013) use a model that combines a power-law with a Gaussian, which requires five-to-six fitting parameters. These choices, however, seem to have little power to constrain the one-halo term of the quasar HOD as KO12 and Shen et al. (2013) derive consistent satellite fractions using their two different HOD parameterizations. Much of this degeneracy regarding the form of the quasar HOD is driven by sizeable uncertainties in the parameters that are fit to model quasar clustering on small scales. It is likely, then, that much larger samples of quasar pairs with small separations, or alternative approaches to deriving the Mean Occupation Function of quasars (e.g. Chatterjee et al. 2013), will be needed to probe the overall statistics of how quasars occupy individual haloes.

Despite the range of possible forms for the Mean Occupation Function of quasars, it remains important to provide empirical constraints on the quasar HOD. Large surveys such as the quasar component (Myers et al. 2015) of the *extended Baryon Oscillation Spectroscopic Survey* (Dawson et al. 2016) and surveys with the *Dark Energy Spectroscopic Instrument* (DESI Collaboration et al. 2016a,b) are beginning to use quasars to constrain the cosmological world model at moderate redshift via redshift-space distortions and the Baryon Acoustic Oscillation scale. Sophisticated simulations are required to model these cosmological constraints, which require an assumed form for the quasar HOD on small scales (e.g. Rodríguez-Torres et al. 2017). Recently, we assembled by far the largest sample of quasar pairs that can be used to probe quasar clustering on scales of a few dozen kiloparsecs, well into the one-halo regime (Eftekhari et al. 2017). In this paper, we combine the sample of Eftekhari et al. (2017) with other clustering results on larger scales (e.g. Kayo & Oguri 2012; Laurent et al. 2017) to provide the best current constraints on the quasar HOD.

This paper is structured as follows: §2 summarizes the prop-

erties of the samples that are used in small and large scale clustering measurements. The measurements themselves are detailed in §3, the modeling approach and the chosen parameterization is described in §4, and ???

We adopt a  $\Lambda$ CDM cosmological model with matter and dark energy and baryon density densities of  $\Omega_m = 0.308$ ,  $\Omega_\Lambda = 0.693$ , and  $\Omega_b = 0.045$ , a Hubble parameter of  $h = 0.678$ , amplitude of matter fluctuations  $\sigma_8 = 0.814$ , and the slope of the initial power spectrum  $n_s = 0.968$ , consistent with Planck Collaboration et al. (2015). All distances quoted throughout the paper are in comoving coordinates unless noted otherwise, denoting the proper coordinates with addition of “p” to the distance units (i.e.,  $h^{-1}$  pkpc or  $h^{-1}$  pMpc).

## 2 DATA

We use two independently compiled samples of confirmed quasars for clustering measurements at kpc and Mpc scales. The small-scale clustering measurement used in this work is drawn from a complete sample of  $g < 20.85$  confirmed quasars at  $z \sim 1.5$  (see Eftekhari et al. 2017) and the large-scale clustering measurement is determined using a sample of  $g < 20.85$  quasars from the extended Baryon Oscillation Spectroscopic Survey (eBOSS; DR14 Dawson et al. 2016; Abolfathi et al. 2018), also at  $z \sim 1.5$ . We apply a number of adjustments prior to measuring the two-point correlation function and combine these two measurements into a single constraint that spans comoving distances of  $\sim 0.01\text{--}100 h^{-1}$  Mpc. In this section of the paper, we summarize the compilation process and properties of the two samples.

### 2.1 KDE-complete sample of close pairs and the associated random catalog

On small scales, we study the “KDE-complete” sample of 47 spectroscopically confirmed “binary” quasars from Eftekhari et al. (2017), which have angular separations of  $2.9'' \leq \theta \leq 7.7''$  over a redshift range of  $0.43 \leq z \leq 2.2$ . The target sample from which these 47 spectroscopically confirmed “binaries” was drawn is 1,172,157 high-probability quasar candidates compiled by applying a Kernel Density Estimation technique (KDE; Richards et al. 2004) to all the point sources in Data Release 6 of the SDSS (Adelman-McCarthy et al. 2008) imaging data down to  $i = 21.3$ . A total of 290,694 quasar candidates at  $0.43 \leq z \leq 2.2$  was selected via a non-parametric Bayesian classifier with  $\sim 92.7\%$  efficiency (see Eftekhari et al. 2017, and references therein for details). A carefully designed long-slit spectroscopic campaign observed a homogeneous subsample of these pair candidates over the course of three years (see Table 1 of Eftekhari et al. 2017).

Of the 47 pairs in the KDE-complete sample (presented in Figure 4 and Table 5 of Eftekhari et al. 2017), 44 reside in the selected redshift range for our current study ( $0.8 \lesssim z \lesssim 2.2$  with  $\bar{z} \sim 1.5$ ). The comoving separations of quasars in these pairs span  $43.3 \lesssim r_p \lesssim 92.3 h^{-1}$  kpc. We use this sample to make our sub-Mpc quasar clustering measurement, creating a random catalog as outlined in section 3.1 of Eftekhari et al. (2017).

### 2.2 eBOSS quasars with $g < 20.85$ and the associated random catalog

To produce a “Mpc-scale” clustering measurement, we use a large sample of spectroscopically confirmed quasars from the extended

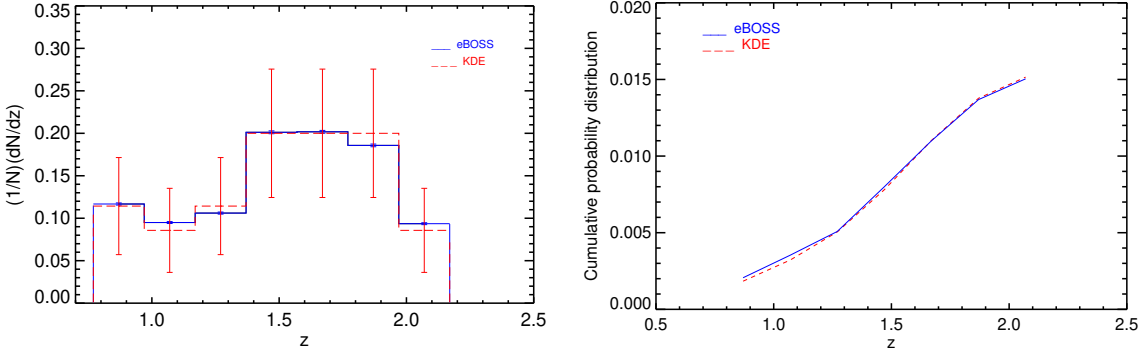


**Figure 1.** Right: Normalized redshift distribution of the KDE-complete sample of ( $< 7''$ ) pairs (dashed red line) and the down-sampled redshift distribution of the eBOSS quasars (solid blue line). The “downsampling” process was performed to match the redshift distribution of the KDE-complete and eBOSS quasars in order to jointly model their clustering measurements (see §2). Left: the cumulative distribution function (CDF) of our KDE and eBOSS samples.

| $z_{\text{min}}$ | $z_{\text{mid}}$ | $z_{\text{max}}$ | $(1/N_{\text{eBOSS}}) dN/dz$ | Error | $(1/N_{\text{KDE}}) dN/dz$ | Error |
|------------------|------------------|------------------|------------------------------|-------|----------------------------|-------|
| 0.77             | 0.87             | 0.97             | 0.117                        | 0.001 | 0.114                      | 0.057 |
| 0.97             | 1.07             | 1.17             | 0.095                        | 0.001 | 0.086                      | 0.049 |
| 1.17             | 1.27             | 1.37             | 0.106                        | 0.001 | 0.114                      | 0.057 |
| 1.37             | 1.47             | 1.57             | 0.201                        | 0.002 | 0.200                      | 0.076 |
| 1.58             | 1.67             | 1.77             | 0.202                        | 0.002 | 0.200                      | 0.076 |
| 1.77             | 1.87             | 1.97             | 0.186                        | 0.002 | 0.200                      | 0.076 |
| 1.97             | 2.07             | 2.17             | 0.094                        | 0.001 | 0.086                      | 0.049 |

**Table 1.** Normalized distribution of the spectroscopic redshifts of quasars in eBOSS (4th column) and the KDE-complete sample of close pairs (6th column) in the redshift bins depicted in Fig. 1.

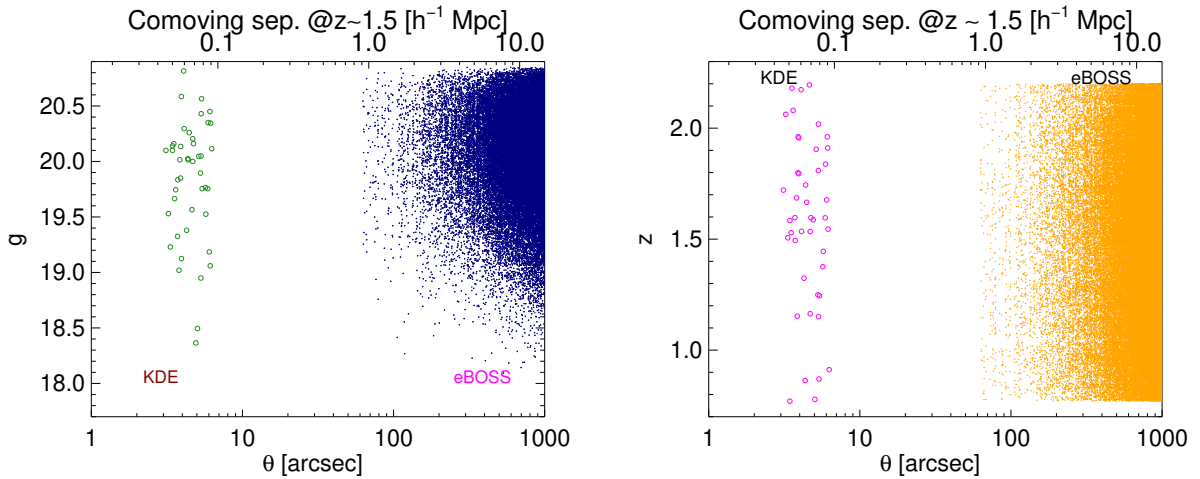


**Figure 2.** Angular separation of quasars in each of the pairs that are used for the small and large-scale clustering measurement as a function of their  $g$ -magnitudes (left) and their redshifts (right). Blue dots and green circles in the left-hand panel and orange dots and pink circles in the right-hand panel each represent one quasar pair. The open circles in both panels represent the 44 ( $< 7''$ ) pairs drawn from our KDE-complete “parent sample” of 243,110 quasar candidates (see Eftekhari et al. 2017, for details). The blue and orange dots in the left-hand and right-hand panels are the quasar pairs in a sample of 39,083  $g \leqslant 20.85$  quasars from eBOSS. For consistency, we applied the same magnitude and redshift limits to both samples. The comoving transverse separation at the average redshift of both samples ( $z \sim 1.5$ ) is included as the top axis in each panel.

Baryon Oscillation Spectroscopic Survey (eBOSS; Dawson et al. 2016) targeted as described in Myers et al. (2015). We begin with a set of 116,866 eBOSS quasars (released in SDSS-DR14; Abolfathi et al. 2018) and its associated  $\sim 44 \times$  larger random catalog. The random catalog models variations in the completeness of eBOSS quasars across the survey footprint and mocks the number density and redshift distribution of the targets (see, e.g. Swanson et al. 2008; Laurent et al. 2017).

The eBOSS random catalogs that we adopt are similar to those used in Laurent et al. (2017) and Rodríguez-Torres et al. (2017), which include weights to correct for incompleteness in identifying quasars. Corrections include a depth-dependent systematic weight ( $w_{sys}$  : WEIGHT\\_SYSTOT), a weight to account for redshift failures ( $w_{zf}$  : WEIGHT\\_NOZ), and a fiber collision ( $w_{cp}$  : WEIGHT\\_CP) term (see Anderson et al. 2012; Ross et al. 2012; Bianchi & Percival 2017, for more details regarding how weights are determined). The total weight for each quasar is ultimately defined as  $w_{qso} = w_{fkp}w_{sys}(w_{zf} + w_{cp} - 1)$  where  $w_{fkp}$  : (WEIGHT\\_FKP) is designed to optimally estimate the two point correlation function (see Feldman, Kaiser & Peacock 1994).

Due to the size of the ferrules that support the fibers that feed the eBOSS spectrographs, eBOSS cannot place fibers closer than  $62''$ , except in regions where multiple spectroscopic plates overlap (Dawson et al. 2016). To measure clustering on small scales, it is critical to be complete as the interplay between the fiber collision radius and the *unknown* small-scale clustering of the targets is impossible to perfectly reconstruct because quasar samples are sparse enough that the number of collided pairs is very small (e.g., Rodríguez-Torres et al. 2017). As the  $62''$  eBOSS angular separation limit is equivalent to a comoving separation of  $0.92 h^{-1}\text{Mpc}$  at  $z \sim 1.5$ , throughout the current paper we set the first bin of comoving separation at which we start to measure our “Mpc-scale” two-point correlation function (2PCF), to be  $1.1 h^{-1}\text{Mpc}$  to ensure that we are on scales larger than the fiber-collision limit. See Guo, Zehavi & Zheng (2012) and Hahn et al. (2017) for detailed analyses of the efficiency of fiber collision corrections at small scales.

### 2.3 Matching quasar samples in luminosity and redshift

A total of 88,764 of the quasars discussed in §2.2 fall in the redshift range  $0.8 \lesssim z \lesssim 2.2$ , of which 40,821 also have  $g < 20.85$ , matching the redshift and brightness limits for the quasar pairs in the KDE-complete sample discussed in §2.1. Maintaining a similar redshift and luminosity range for quasars in both our “KDE-complete” and “Mpc-scale” samples would be ideal to guarantee that our clustering measurement studies a consistent population of quasars across all scales, although any luminosity evolution in quasar clustering should be small in the regime we consider (e.g. Shen et al. 2007; Allevato et al. 2011; Shen et al. 2013; Allevato et al. 2014; Eftekhazadeh et al. 2015; McGreer et al. 2016).

We match the distributions by *downsampling* the much larger eBOSS quasar sample in over-populated redshift bins to that of the KDE-complete sample of close pairs, by first determining the over population at each bin of redshift and then randomly removing the *extra* number of targets from that redshift bin. Figure 1 shows the normalized redshift distribution of the KDE-complete sample of ( $< 7''$ ) pairs and the down-sampled and matched redshift distribution of the eBOSS quasars. The left-hand-side of this figure illustrates the cumulative probability distribution function (CDF) of the KDE and eBOSS samples. The two-sample Kolmogorov-Smirnov test shows that the probability that these two samples are drawn from the same distribution is 86%. The errors on the redshift distribution

of the KDE sample are Poisson errors to show that the match is well within the one-sigma uncertainty. We provide the resulting matched redshift distributions of the KDE-complete sample of 44 pairs and the 33,245 eBOSS  $g < 20.85$  quasars in Table 1.

Figure 2 shows the angular separation of quasars in each of the pairs that we use for the small- and large-scale clustering measurement as a function of their g-magnitudes and their redshifts. As is evident in Fig. 2, both sets of pairs from the small and large angular separations exhibit similar distributions in magnitude and redshift. As noted in §2.2, fiber-collision-effects impose a lower limit of  $62''$  for the angular separation of the quasar pairs. This produces a  $\sim 55''$  gap between the close pairs from the KDE-complete sample at  $7''$  and the eBOSS pairs.

## 3 CLUSTERING MEASUREMENT

In this section, we summarize how we use the samples outlined in §2 to make quasar clustering measurements at  $z \sim 1.5$  on kpc and Mpc scales.

### 3.1 kpc-scale clustering

The method we adopt for measuring the volume-averaged correlation function in real space with sparse samples of close pairs is discussed in Eftekhazadeh et al. (2017) and Hennawi et al. (2006). Fig. 2 of Eftekhazadeh et al. (2017) shows how the sample of 47 pairs with angular separations of  $< 7''$  that we outlined in §2.1 constitute a complete sample and how they populate the redshift-physical-separation plane. We follow the method depicted in Fig. 2 of Eftekhazadeh et al. (2017) but apply an additional redshift cut of  $0.8 \lesssim z \lesssim 2.2$  to mirror the eBOSS sample that we will use to measure quasar clustering on Mpc-scales. This results in a sample of 44 pairs that are complete across a range of proper scales, which we convert to comoving coordinates.

We show the measured volume-averaged correlation function ( $\bar{W}_p$ ) for the resulting 44 pairs of quasars in 4 bins of separation in Fig. 3. As each quasar pair is only counted once (i.e. is independent), we adopt Poisson errors from Gehrels (1986) for the uncertainty of the measured  $\bar{W}_p$ . The volume-averaged correlation function was measured for 6, 13, 12 and 13 quasar pairs in four bins of separation at comoving average separations of 48, 58, 70 and  $85 h^{-1}\text{kpc}$ , respectively. Similarly to the measurement presented in Eftekhazadeh et al. (2017), we also measure  $\bar{W}_p$  for the full bin of  $43.4$  to  $92.3 h^{-1}\text{kpc}$  (shown as a single bin at  $\bar{r}_p = 67.8 h^{-1}\text{kpc}$  in the right-hand panel of Fig. 3). The process through which the *expected* Quasar-Random pairs (i.e. the random catalog needed to calibrate clustering),  $\langle QR \rangle$ , is calculated is detailed in Eftekhazadeh et al. (2017).

The volume-averaged correlation function,  $\bar{W}_p$ , is useful in characterizing quasar clustering on small scales, as close quasar pairs are scarce. Quasar clustering is more typically *modeled*, however using the projected correlation function (i.e.,  $w_p(r_p) = 2 \int_0^\infty d\pi \xi(\pi, r_p)$ ). We therefore convert  $\bar{W}_p$  to the equivalent  $w_p(r_p)$  to make it easier to compare our measurements to HOD models. We use the approximation:

$$\bar{W}_p(r_p) \sim \frac{1}{N_{qso}} \int_{z_{min}}^{z_{max}} dz \frac{dV_c}{dz} n(z) \frac{1}{v_z} \int_0^{v_z} d\pi \xi(\sqrt{(r_p^2 + \pi^2)}, z), \quad (1)$$

where  $n(z)$  is the comoving number density of quasars in bins

of redshift,  $v_z \equiv v_{max}(1+z)/H(z)$ ,  $v_{max} = 2000 \text{ km s}^{-1}$ ,  $H(z)$  is the expansion rate at redshift  $z$ ,  $N_{qso} \sim \int_{z_{min}}^{z_{max}} dz \frac{dV}{dz} n(z)$  and  $\int_0^{v_z} d\pi \xi(\sqrt{(r_p^2 + \pi^2)}, z)$  is essentially  $w_p(r_p, v_z \rightarrow \infty)$ . We model the correlation function  $\xi(r)$  as a two-parameter power-law  $(\frac{r}{r_0})^{-\gamma}$  with  $\gamma \sim -2.0$  and  $r_0 = 5.0 \text{ h}^{-1} \text{ Mpc}$ , as in Eftekharzadeh et al. (2017). A similar approximation to Eqn. 1 with a different numerical approach was used in KO12 to convert  $\bar{W}_p(r_p)$  to  $w_p(r_p)$ .

### 3.2 Mpc-scale clustering

We calculate the Mpc-scale section of the correlation function using the sample of eBOSS quasars described in §2.3 that have been down-sampled to match the number density of the KDE parent sample with which the kpc-scale correlation function is measured ( $\sim 6.462 \times 10^{-6} \text{ h}^3 \text{ Mpc}^{-3}$ ). The corresponding random catalog for the down-sampled quasar catalog is created by keeping track of the fraction ( $f$ ) of objects that are brighter than  $g = 20.85$  in each bin of redshift. For each object in the original random catalog and its assigned redshift, if a random number between 0 and 1 is less than  $f$ , then that object is retained, otherwise it is discarded. We calculate  $w_p(r_p)$  using the estimator of Landy & Szalay (1993). As discussed in §2.2, the quasars that are counted in the Quasar-Random and Quasar-Quasar pairs, have an associated weight  $w_{qso}$ , which we apply to the pair counts. The measured correlation function in bins of comoving separation across  $1 < r_p < 100 \text{ h}^{-1} \text{ Mpc}$  are shown with filled black circles in Fig. 3, Fig. 4 and Fig. 5. The error bars are calculated through a jackknife resampling (see, e.g., eqn. 4 of Eftekharzadeh et al. 2015).

## 4 HOD MODELLING

One important application of measuring the real-space correlation function of a given population is to provide the statistics of how those objects populate individual dark matter haloes. The Halo Occupation Distribution framework provides the average number of objects residing within one halo (i.e.,  $\langle N(M) \rangle$ ) as well as an analytical form for their distribution in each halo under the assumption that  $\langle N(M) \rangle$  is a function of the halo mass (Peacock & Smith 2000; Seljak 2000; Scoccimarro et al. 2001; Berlind & Weinberg 2002). Variations of this modelling approach have been used for interpreting the measured correlation function of Active Galactic Nuclei (AGNs) and quasars in recent years (e.g., Porciani, Magliocchetti & Norberg 2004; Coil et al. 2004; Abazajian et al. 2005; Coil et al. 2006, 2007, 2009; Miyaji et al. 2011; Richardson et al. 2012; Kayo & Oguri 2012; Krumpe et al. 2012; Richardson et al. 2013; Shen et al. 2013; Coil et al. 2016, 2017).

Although several studies have attempted to constrain HOD parameters for quasars on both large and small scales, measured quasar correlation functions on halo scales ( $< 1 \text{ h}^{-1} \text{ Mpc}$ ) are rare, and so HOD modeling of the correlation function on these scales has been limited. In this paper, We adopt an HOD approach similar to KO12, which modelled quasar clustering over a similar scale and redshift regime to our current work.

The projected two-point correlation function can be modeled using the matter power spectrum (see, e.g., Cooray & Sheth 2002):

$$w_p(r_p) = \int_0^\infty \frac{k dk}{2\pi} P(k) J_0(kr_p), \quad (2)$$

where  $J_0$  is the zeroth order of the Bessel function of the first kind.

The power spectrum  $P(k)$  can be separated into two independent *one-* and *two-halo* terms:

$$P(k) = P_{1h}(k) + P_{2h}(k). \quad (3)$$

The two-halo term can be simply obtained by

$$P_{2h}(k) = b^2 P_{lin}(k), \quad (4)$$

where the linear matter power spectrum,  $P_{lin}$  is computed using Eisenstein & Hu (1999)'s fitting form with our chosen cosmological parameters and  $b$  is the bias parameter that can be modeled as:

$$b = \frac{\int b_h(M) \frac{dn}{dM} dM}{\int \frac{dn}{dM} dM}. \quad (5)$$

Following a commonly assumed mass-dependence, we model the mean number of occupying quasars in individual haloes as a three-parameter Gaussian:

$$\langle N(M) \rangle = f_N \times \frac{1}{\sqrt{(2\pi)\Delta_m}} \exp\left[-\frac{\ln^2(M/M_m)}{2\Delta_m^2}\right], \quad (6)$$

where  $M_m$  is the minimum mass for a dark matter halo that can host a quasar and  $\Delta_m$  is the width of the initial mass distribution.  $f_N$  is the normalization factor that matches the observed number density of the quasars in our sample ( $\sim 6.462 \times 10^{-6} \text{ h}^3 \text{ Mpc}^{-3}$ ) with its expected value from the halo mass function and the assumed distribution of haloes. In the one-halo regime, the correlation function is measured using pairs of haloes that lie within the boundaries of individual haloes themselves. Therefore, in this regime, assumptions have to be made regarding the fraction of quasars that exist as a “satellite” of a central quasar ( $f_{sat}$ ), and regarding the fraction of quasars that reside at the center of dark matter haloes ( $p$ ). The halo occupation model then has “central” and “satellite” components such that  $\langle N_{cen}(M) \rangle = (1 - f_{sat})\langle N(M) \rangle$  and  $\langle N_{sat}(M) \rangle = f_{sat}\langle N(M) \rangle$  (Berlind & Weinberg 2002; Kravtsov et al. 2004; Zheng et al. 2005). KO12 justifies ignoring the mass dependence of the satellite fraction (i.e.,  $f_{sat}(M) \simeq f_{sat}$ ) by choosing a relatively narrow ( $\sim 2$  dex) range for the halo mass distribution around the characterized minimum mass,  $M_m$ . Similar to their approach, we assume a constant satellite fraction and investigate any difference by relaxing the width of the halo mass distribution,  $\Delta_m$ , as an additional fitting parameter in our HOD model.

We further adopt an “independent quasar activity” assumption for the central and satellite quasars. This facilitates the use of Poisson statistics for the integrator in the description of the one-halo term of the power spectrum used in KO12 (see also Seljak 2000):

$$\begin{aligned} P_{1h}(k) &= \frac{1}{n_q^2} \int \langle N(N-1) \rangle u(k, M)^p \frac{dn}{dM} dM \\ &\equiv 2\langle N_{cen} N_{sat} \rangle u(k, M) + \langle N_{sat}(N_{sat}-1) \rangle |u(k, M)|^2 \\ &= [2f_{sat}(1-f_{sat})u(k, M) + f_{sat}^2|u(k, M)|^2]\langle N(M) \rangle, \end{aligned} \quad (7)$$

where  $u(k, M)$  is the Fourier transform of the quasar number density profile in a dark matter halo of mass  $M$ . We adopt an NFW profile (Navarro, Frenk & White 1997) with concentration parameter

$$c(M, z) = \frac{c_0}{1+z} \left[ \frac{M}{M^*} \right]^{-0.13}, \quad (8)$$

where  $M^*$  is the nonlinear mass scale for collapse at  $z = 0$  (Cooray

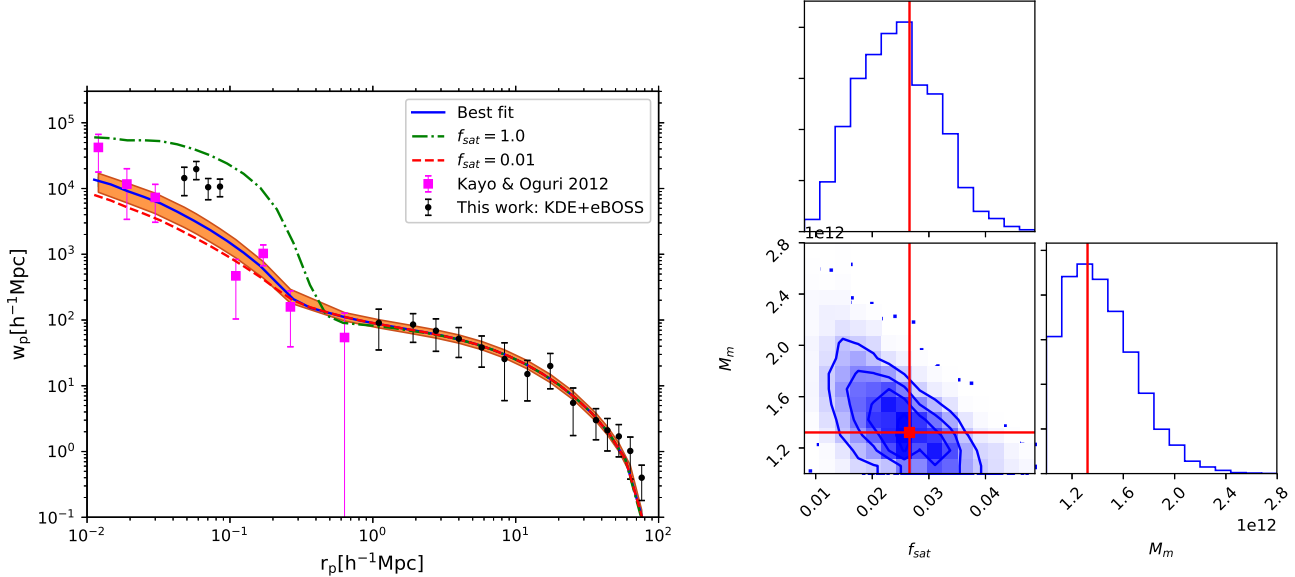


**Figure 3.** Left: Our HOD prediction of the projected correlation function that best-fits the observational data. The solid blue curve is the best-fit and the red dashed and green dotted-dashed lines are the model with best-fit  $M_m$  but  $f_{sat} = 0.01$  and  $f_{sat} = 1.0$ . We verified that relaxing  $\Delta_m$ , as the third parameter, has no significant effect on the shape of the best-fit model. The best-fit value for  $\Delta_m$  stays consistent with 0.75 that was derived independently by KO12. The shaded envelope around the best fit model is the extent of the 2-sigma certainty for the shape of the HOD model at each bin of the projected distance ( $r_p$ ). All the data points depicted here (filled pink squares from KO12 and filled black circles) have participated in the fit. See §2 for a description of the clustering measurement from two separate sets of observations at  $z \sim 1.5$  at small (kpc) and large (Mpc) scales. Best fit model has  $M_m = 1.43^{+0.31}_{-0.23} \times 10^{12} h^{-1} M_\odot$ , and  $f_{sat} = 0.0244^{+0.0075}_{-0.0070}$  with  $\chi^2_{red} = 1.46$ . Right: The result of the 2-parameter Monte-Carlo fit to the projected two point correlation function over  $\sim 0.01 - 100 h^{-1}\text{Mpc}$  for the model shown in the left. Diagonal panels show the probability distribution functions (PDFs) of the fitting parameters (i.e., satellite fraction ( $f_{sat}$ ), minimum halo mass that hosts a quasar ( $M_{min}$ ), and the range of the halo masses that quasars occupy ( $\Delta_m$ )). The off-diagonal panels show the density contours of the chosen sets of HOD parameters within one to three-sigma certainties. As the Marcov Chain explores the parameter space for each of the fitting parameters, each step of the chain takes a random walk with a randomly chosen step size and calculates the likelihood of the new set of parameters based on the difference between their deduced chi-squared and that of the previous set of chosen parameters.

& Sheth 2002). In this work, we initially chose  $c_0 = 9$  and investigated the change in the best-fit parameters for a model with haloes with 10 times higher concentration (see the right panel of Fig. 5). A weak dependency of the HOD model on the concentration parameter is reported by a number of studies (Richardson et al. 2012, 2013; Shen et al. 2013) that used a different HOD formalism where the distribution of the central and satellite haloes are assumed to be a softened three-parameter step function and a two-parameter power-law respectively. We further discuss the differences between our chosen parameters and those previously used in the literature in §5 where we summarize the differences between assumptions and their potential effect on the best-fit parameters.

## 5 RESULTS AND DISCUSSION

We fit our HOD model to the available clustering measurements using a variety of data combinations including and excluding seven to eight bins of the measured correlation function from KO12 (the filled pink squares in Fig. 3, Fig. 4 and Fig. 5). Note that the samples used in KO12 match our sample reasonably well in number density ( $\sim 1.35 \times 10^{-6} h^3 \text{Mpc}^{-3}$ ) and average redshift ( $z \sim 1.4$ ). Assuming that quasars do not evolve rapidly over the timescales that correspond to  $\Delta z \sim 0.1$  and that clustering does not evolve strongly with luminosity from the KO12 sample to our sample. (do

we know this for a fact? KDE sample has targets down to  $i=23$  but Kayo and Oguri 2012 sample has quasars down to  $i=20$ ), we used their data to fill the gap between our small- and large-scale measurements. We examined the effect of using the four binned correlation function or using the single-binned measurements in the best fit parameters (see Fig. 3 and Fig. 4). Table 2 summarizes the fitting results for all the fitting trials.

Influenced by the parameterization used in KO12, we investigated relaxing  $\Delta_m$  as the third parameter for the HOD model (in addition to  $f_{sat}$  and  $M_m$ ) and found it to have no significant effect on the best-fit model. We also examined the best-fit quality of an HOD model with 10 times higher average concentration parameter ( $10 \times \bar{c}$ ) to the full-scale correlation function (with and without including KO12's measurement in the fit). Figure 5 shows a steeper one-halo term for the best-fit model that is more in accord with the measured correlation function by KO12. But this *shape change* produces best-fit parameters that are consistent with haloes that do not have a  $10 \times$  higher concentration (see the second and the third rows of Table 2).

To remove the added assumptions for including past measurements in the results, we fit the same two-parameter HOD model used in prior fitting processes only to our data from the KDE-complete and eBOSS samples, leaving data from KO12 out of the fit. The solid blue line in Figure 6 represents the best-fit to this data (KDE+eBOSS). The solid dark red model is the best-fit

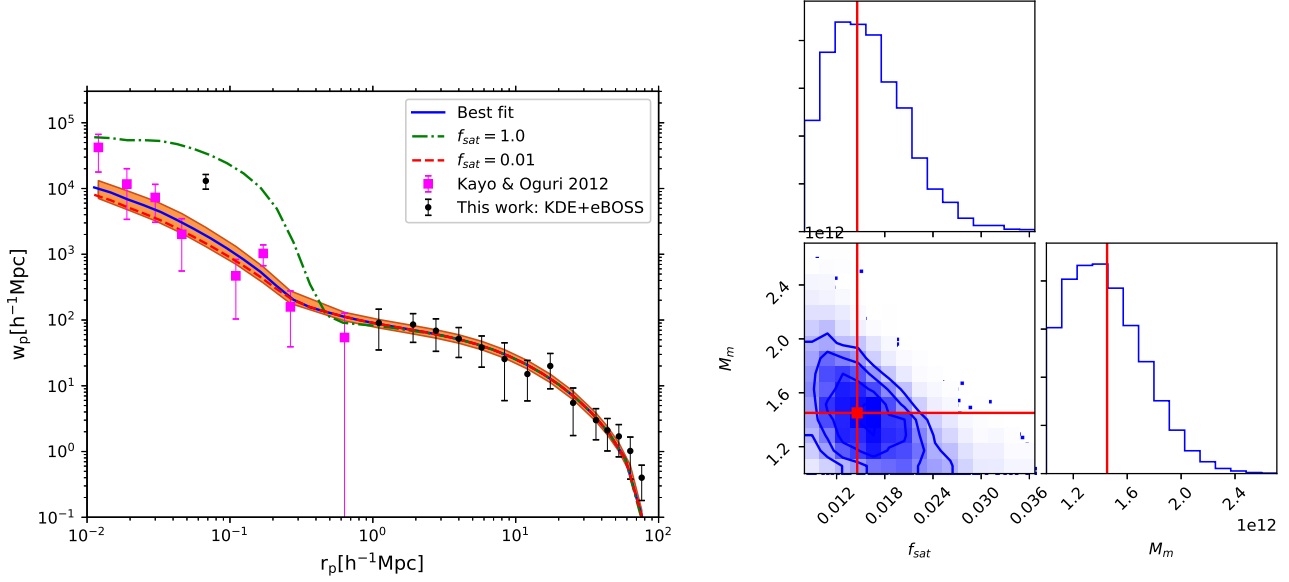


**Figure 4.** Left: Similar to the right panel of Fig. 3 but for a single bin of the measured correlation function using the KDE-complete sample of close pairs. Best fit model (solid blue curve) has  $M_m = 1.45^{+0.32}_{-0.25} \times 10^{12} h^{-1} M_\odot$ , and  $f_{\text{sat}} = 0.016^{+0.005}_{-0.004}$  with reduced  $\chi^2 = 1.18$ . The shaded envelope around the best fit model is the extent of the 2-sigma certainty for the shape of the HOD model at each bin of the projected distance ( $r_p$ ). Right: Fitting statistics similar to the one shown for the fitting process in the right-hand panel of Fig. 3.

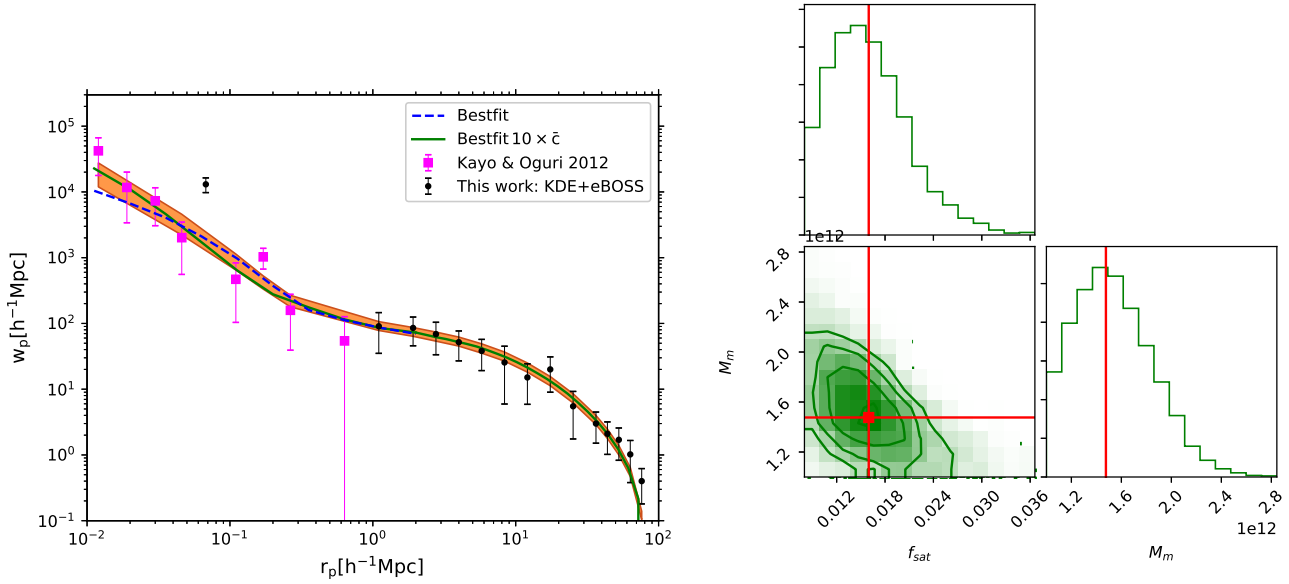


**Figure 5.** Left: Our HOD prediction of the projected correlation function that best-fits the full-scale measurement (all the shown data points participated in the best-fit determination) and where the dark matter haloes are assumed to have 10 times higher average concentrations than the best-fit model shown with the dashed blue line (solid blue curve in Fig. 4). The best-fit model (solid green line) has  $M_m = 1.55^{+0.35}_{-0.29} \times 10^{12} h^{-1} M_\odot$ , and  $f_{\text{sat}} = 0.016^{+0.005}_{-0.004}$  with reduced  $\chi^2 = 1.213$ . The shaded envelope around the best-fit model is the extent of the 2-sigma certainty for the shape of the HOD model at each bin of the projected distance ( $r_p$ ). Although the steeper shape of the one-halo term seems to better follow the measurements reported in small scales, the fitting results do not show a significantly better constraint on the fitting parameters.

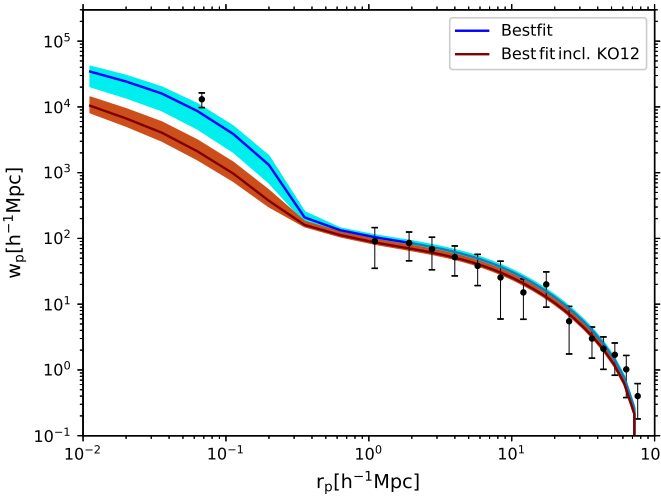


**Figure 6.** Left: Our HOD prediction of the projected correlation function that best-fits the full-scale measurement where only the measurement from KDE-complete sample of close pairs and the data from eBOSS clustering is added (solid blue curve in Fig.4). The best-fit model has  $M_m = 2.32_{-0.440}^{+0.463} \times 10^{12} h^{-1} M_\odot$ , and  $f_{\text{sat}} = 0.062_{-0.026}^{+0.028}$  with reduced  $\chi^2 = 1.09$ . The shaded envelope around the best-fit model is the extent of the 1-sigma certainty for the shape of the HOD model at each bin of the projected distance ( $r_p$ ).

model to the same KDE+eBOSS measurements but also the measured  $w_p$  over eight bins of comoving distance from KO12. The shaded envelopes that represent the  $1-\sigma$  uncertainties for the best-fit models, are visibly separated. This indicates that inclusion of the clustering measurement at  $z \sim 1.4$  results in a significantly different best-fit (see the second and the last row of Table 2). The lower clustering signal measured for quasars in the KO12 sample results in a satellite fraction that is  $> 30\times$  smaller than what is measured for our KDE-complete sample. However, our best-fit  $f_{\text{sat}} = 0.062_{-0.026}^{+0.028}$  is consistent with the reported value from KO12 of  $f_{\text{sat}} = 0.048_{-0.015}^{+0.016}$  for an NFW profile.

Recent HOD analysis of the local AGNs at  $z \sim 0.01 - 0.1$  has revealed that AGNs reside in similar dark matter haloes to that of galaxies with similar stellar mass (reference a recent analysis with BASS-2MASS CCF measurement at  $z=0.01-0.1$  using HALOTOOLS package). This could be interpreted as a by product of observing no significant luminosity dependency of quasar and AGN clustering.

A look at the recent investigations on the effective environmental factors that lead to presence of two AGN types and the contradictory findings on the difference between their bias with respect to dark matter, halo mass, black hole mass, mean number of satellites (see, e.g., DiPompeo et al. 2015, 2017; Krumpe et al. 2018) is a shining evidence of the need for theoretical followup and pairing up the measured correlation function with complementary measurements that enhances the presence of the observationally challenging bins at kpc scales (see, Starikova et al. 2011, for a proposed alternative).

In recent years, an increasing number of reports on the persistent degeneracies between the best-fit parameters of widely used HOD formalism (initially designed for local AGNs) have emerged (Coil et al. 2016, 2017).

These studies differ from this work (as well as KO12) in two significant ways: (i) The two-point correlation function in those

studies fall short of measurements over scales well within individual halo ( $\sim 10 - 100 h^{-1} \text{kpc}$ ) where the one-halo term of the power spectrum has an ideal chance of constraining with observation. (ii) This work (and KO12) assumes a Gaussian form for distribution of both central and satellite haloes while power-law distribution has been assumed for the satellite fraction (see, e.g., Zheng, Coil & Zehavi 2007; Coil et al. 2009; Allevato et al. 2012; Richardson et al. 2012, 2013; Krumpe et al. 2018). Our simple HOD model suggests a constant satellite fraction for when the average occupants grows rapidly within narrow range of host halo mass which describes the excess clustering in subhalo scales (Kayo & Oguri 2012). Assuming similar distribution for centrals and satellite quasars indicates the independency of the two population to the point that satellites could be quasars while the central galaxy is not a quasar. A gaussian distribution for the subhalo population does not contradict attribution of the excess clustering to merger that has been suggested in small scale clustering analysis for quasars (e.g., Hennawi et al. 2006; Myers et al. 2008) or the presented merger tree of a dark matter halo across discrete time steps from simulation snapshots (Giocoli, Tormen & van den Bosch 2008; Giocoli, Pieri & Tormen 2008; Giocoli et al. 2010). Shen et al. (2013) performed a comprehensive investigation of the formalism introduced by Zheng et al. (2005) and implemented by a number of clustering analysis ever since (Zheng, Coil & Zehavi 2007; Miyaji et al. 2011; Zehavi et al. 2011; Richardson et al. 2012, 2013)(add more refs) by performing a five and six parameter fit to their galaxy-quasar cross correlation function at  $\bar{z} \sim 0.5$ .

## ACKNOWLEDGMENTS

SE and ADM acknowledge support by the National Science Foundation through grant number 1616168.

Funding for the Sloan Digital Sky Survey IV has been provided by the Alfred P. Sloan Foundation, the U.S. Department of Energy Office of Science, and the Participating Institutions. SDSS acknowledges support and resources from the Center for High-Performance Computing at the University of Utah. The SDSS web site is <http://www.sdss.org>.

SDSS is managed by the Astrophysical Research Consortium for the Participating Institutions of the SDSS Collaboration including the Brazilian Participation Group, the Carnegie Institution for Science, Carnegie Mellon University, the Chilean Participation Group, the French Participation Group, Harvard-Smithsonian Center for Astrophysics, Instituto de Astrofísica de Canarias, The Johns Hopkins University, Kavli Institute for the Physics and Mathematics of the Universe (IPMU) / University of Tokyo, Lawrence Berkeley National Laboratory, Leibniz Institut für Astrophysik Potsdam (AIP), Max-Planck-Institut für Astronomie (MPIA Heidelberg), Max-Planck-Institut für Astrophysik (MPA Garching), Max-Planck-Institut für Extraterrestrische Physik (MPE), National Astronomical Observatories of China, New Mexico State University, New York University, University of Notre Dame, Observatorio Nacional / MCTI, The Ohio State University, Pennsylvania State University, Shanghai Astronomical Observatory, United Kingdom Participation Group, Universidad Nacional Autónoma de México, University of Arizona, University of Colorado Boulder, University of Oxford, University of Portsmouth, University of Utah, University of Virginia, University of Washington, University of Wisconsin, Vanderbilt University, and Yale University.

| Data                                       | $M_m (\times 10^{12} h^{-1} M_\odot)$ | $f_{sat}$                 | $\chi^2_{red}$ (d.o.f) |
|--|---------------------------------------|---------------------------|------------------------|
| 4KDE+14eBOSS+7KO12                         | $1.43^{+0.31}_{-0.25}$                | $0.024^{+0.007}_{-0.007}$ | 1.460 (22)             |
| 1KDE+14eBOSS+8KO12                         | $1.45^{+0.32}_{-0.25}$                | $0.016^{+0.005}_{-0.004}$ | 1.180 (20)             |
| 1KDE+14eBOSS+8KO12 ( $10 \times \bar{v}$ ) | $1.55^{+0.35}_{-0.29}$                | $0.016^{+0.005}_{-0.004}$ | 1.213 (20)             |
| 1KDE+14eBOSS                               | $2.32^{+0.46}_{-0.44}$                | $0.062^{+0.028}_{-0.026}$ | 0.855 (12)             |

**Table 2.** Summary of the fitting results using different data that participated in the fit. The second and third columns are the best-fit parameters and their  $1-\sigma$  uncertainties. The last column lists the reduced  $\chi^2$  (and the degrees of freedom).

## REFERENCES

- Abazajian K. et al., 2005, ApJ, 625, 613  
 Abolfathi B. et al., 2018, ApJS, 235, 42  
 Adelman-McCarthy J. K. et al., 2008, ApJS, 175, 297  
 Allevato V. et al., 2011, ApJ, 736, 99  
 Allevato V. et al., 2014, ApJ, 796, 4  
 Allevato V. et al., 2012, ApJ, 758, 47  
 Anderson L. et al., 2012, MNRAS, 427, 3435  
 Berlind A. A., Weinberg D. H., 2002, ApJ, 575, 587  
 Bianchi D., Percival W. J., 2017, MNRAS, 472, 1106  
 Bolton A. S., Burles S., Schlegel D. J., Eisenstein D. J., Brinkmann J., 2004, AJ, 127, 1860  
 Chatterjee S., Nguyen M. L., Myers A. D., Zheng Z., 2013, ApJ, 779, 147  
 Coil A. L. et al., 2004, ApJ, 609, 525  
 Coil A. L. et al., 2009, ApJ, 701, 1484  
 Coil A. L. et al., 2006, ApJ, 638, 668  
 Coil A. L., Hennawi J. F., Newman J. A., Cooper M. C., Davis M., 2007, ApJ, 654, 115  
 Coil A. L., Mendez A. J., Eisenstein D. J., Moustakas J., 2016, ArXiv:1609.09090  
 Coil A. L., Mendez A. J., Eisenstein D. J., Moustakas J., 2017, ApJ, 838, 87  
 Cooray A., Sheth R., 2002, Phys. Rep., 372, 1  
 Croom S. M., Smith R. J., Boyle B. J., Shanks T., Miller L., Outram P. J., Loaring N. S., 2004, MNRAS, 349, 1397  
 Dawson K. S. et al., 2016, AJ, 151, 44  
 DESI Collaboration et al., 2016a, ArXiv e-prints  
 DESI Collaboration et al., 2016b, ArXiv e-prints  
 DiPompeo M. A., Hickox R. C., Myers A. D., Geach J. E., 2017, MNRAS, 464, 3526  
 DiPompeo M. A., Myers A. D., Hickox R. C., Geach J. E., Holder G., Hainline K. N., Hall S. W., 2015, MNRAS, 446, 3492  
 Eftekharzadeh S., Myers A. D., Hennawi J. F., Djorgovski S. G., Richards G. T., Mahabal A. A., Graham M. J., 2017, MNRAS, 468, 77  
 Eftekharzadeh S. et al., 2015, MNRAS, 453, 2779  
 Eisenstein D. J., Hu W., 1999, ApJ, 511, 5  
 Feldman H. A., Kaiser N., Peacock J. A., 1994, ApJ, 426, 23  
 Folkes S. et al., 1999, MNRAS, 308, 459  
 Fukugita M., Ichikawa T., Gunn J. E., Doi M., Shimasaku K., Schneider D. P., 1996, AJ, 111, 1748  
 Gehrels N., 1986, ApJ, 303, 336  
 Giocoli C., Pieri L., Tormen G., 2008, MNRAS, 387, 689  
 Giocoli C., Tormen G., Sheth R. K., van den Bosch F. C., 2010, MNRAS, 404, 502  
 Giocoli C., Tormen G., van den Bosch F. C., 2008, MNRAS, 386, 2135  
 Gunn J. E. et al., 1998, AJ, 116, 3040  
 Guo H., Zehavi I., Zheng Z., 2012, ApJ, 756, 127  
 Hahn C., Scoccimarro R., Blanton M. R., Tinker J. L., Rodríguez-Torres S. A., 2017, MNRAS, 467, 1940  
 Hennawi J. F. et al., 2010, ApJ, 719, 1672  
 Hennawi J. F. et al., 2006, AJ, 131, 1  
 Kauffmann G., Haehnelt M., 2000, MNRAS, 311, 576  
 Kayo I., Oguri M., 2012, MNRAS, 424, 1363  
 Kormendy J., Richstone D., 1995, ARA&A, 33, 581  
 Kravtsov A. V., Berlind A. A., Wechsler R. H., Klypin A. A., Gottlöber S., Allgood B., Primack J. R., 2004, ApJ, 609, 35  
 Krumpe M., Miyaji T., Coil A. L., Aceves H., 2012, ApJ, 746, 1  
 Krumpe M., Miyaji T., Coil A. L., Aceves H., 2018, MNRAS, 474, 1773  
 Landy S. D., Szalay A. S., 1993, ApJ, 412, 64  
 Laurent P. et al., 2017, JCAP, 7, 017  
 McGreer I. D., Eftekharzadeh S., Myers A. D., Fan X., 2016, AJ, 151, 61  
 Miyaji T., Krumpe M., Coil A. L., Aceves H., 2011, ApJ, 726, 83  
 Myers A. D., Brunner R. J., Nichol R. C., Richards G. T., Schneider D. P., Bahcall N. A., 2007a, ApJ, 658, 85  
 Myers A. D., Brunner R. J., Richards G. T., Nichol R. C., Schneider D. P., Bahcall N. A., 2007b, ApJ, 658, 99  
 Myers A. D. et al., 2006, ApJ, 638, 622  
 Myers A. D. et al., 2015, ApJS, 221, 27  
 Myers A. D., Richards G. T., Brunner R. J., Schneider D. P., Strand N. E., Hall P. B., Blomquist J. A., York D. G., 2008, ApJ, 678, 635  
 Navarro J. F., Frenk C. S., White S. D. M., 1997, ApJ, 490, 493  
 Neyman J., Scott E. L., 1974, in IAU Symposium, Vol. 63, Confrontation of Cosmological Theories with Observational Data, Longair M. S., ed., pp. 129–140  
 Neyman J., Scott E. L., Zonn W., 1962, AJ, 67, 583  
 Ostriker J. P., Peebles P. J. E., Yahil A., 1974, ApJ, 193, L1  
 Peacock J. A., Smith R. E., 2000, MNRAS, 318, 1144  
 Planck Collaboration et al., 2015, ArXiv:1502.01589  
 Porciani C., Magliocchetti M., Norberg P., 2004, MNRAS, 355, 1010  
 Richards G. T. et al., 2004, ApJS, 155, 257  
 Richardson J., Chatterjee S., Zheng Z., Myers A. D., Hickox R., 2013, ApJ, 774, 143  
 Richardson J., Zheng Z., Chatterjee S., Nagai D., Shen Y., 2012, ApJ, 755, 30  
 Rodríguez-Torres S. A. et al., 2017, MNRAS, 468, 728  
 Rojas R. R., Vogeley M. S., Hoyle F., Brinkmann J., 2005, ApJ, 624, 571  
 Rood H. J., Page T. L., Kintner E. C., King I. R., 1972, ApJ, 175, 627

- Ross A. J. et al., 2012, MNRAS, 424, 564  
 Ross N. P. et al., 2013, ApJ, 773, 14  
 Ross N. P. et al., 2009, ApJ, 697, 1634  
 Rubin V. C., Thonnard N., Ford, Jr. W. K., 1978, ApJ, 225, L107  
 Scoccimarro R., Sheth R. K., Hui L., Jain B., 2001, ApJ, 546, 20  
 Seljak U., 2000, MNRAS, 318, 203  
 Shen Y. et al., 2013, ApJ, 778, 98  
 Shen Y. et al., 2007, AJ, 133, 2222  
 Shen Y. et al., 2009, ApJ, 697, 1656  
 Starikova S. et al., 2011, ApJ, 741, 15  
 Stoughton C. et al., 2002, AJ, 123, 485  
 Strauss M. A. et al., 2002, AJ, 124, 1810  
 Swanson M. E. C., Tegmark M., Hamilton A. J. S., Hill J. C.,  
   2008, MNRAS, 387, 1391  
 Tegmark M. et al., 2004, ApJ, 606, 702  
 Vanden Berk D. E. et al., 2001, AJ, 122, 549  
 West A. A. et al., 2004, AJ, 128, 426  
 White M. et al., 2012, MNRAS, 424, 933  
 White S. D. M., Rees M. J., 1978, MNRAS, 183, 341  
 Wilhite B. C., Vanden Berk D. E., Kron R. G., Schneider D. P.,  
   Pereyra N., Brunner R. J., Richards G. T., Brinkmann J. V., 2005,  
   ApJ, 633, 638  
 Yip C. W. et al., 2004a, AJ, 128, 585  
 Yip C. W. et al., 2004b, AJ, 128, 2603  
 York D. G. et al., 2000, AJ, 120, 1579  
 Zehavi I. et al., 2011, ApJ, 736, 59  
 Zheng Z. et al., 2005, ApJ, 633, 791  
 Zheng Z., Coil A. L., Zehavi I., 2007, ApJ, 667, 760